Appl Nanosci (2011) 1:237–246
DOI 10.1007/s13204-011-0032-1

ORIGINAL ARTICLE

Controlling the optimum dose of AMPTS functionalized-magnetite nanoparticles for hyperthermia cancer therapy

Yosefine Arum · Youngjin Song · Junghwan Oh

Received: 24 May 2011 / Accepted: 12 September 2011 / Published online: 21 October 2011
© The Author(s) 2011. This article is published with open access at Springerlink.com

Abstract Magnetic hyperthermia has been used for many years to treat a variety of malignant tumors. One of the problems in magnetic hyperthermia is the choice of the correct particle concentration to achieve a defined temperature increase in the tumor tissue. In this study, we evaluated magnetic heat distribution induced by Fe_3O_4-APTMS magnetic nanoparticles in agar tissue phantom when it subjected to the AC magnetic filed. Using the correct nanoparticle dosage and considering their specific loss power, it is possible to estimate the efficiency of this therapeutic method. The experimental data were compared with a computer-based model, which were created using COMSOL Multiphysics to simulate the heat dissipation within the tissue for typical configurations of the tumor position as well as particle distribution within the tumor. Heating the cancer cells up to 50°C for 10 min was sufficient for complete cell killing and the heat dose of 19.9 W/g_{tissue} is required for 5-mm tumor. Cell viability assay showed that MNPs exhibited no significant cytotoxicity against HeLa cells. Additionally, it was observed that the FITC-labeled Fe_3O_4-APTMS MNPs presented high cell biocompatibility and cellular uptake for efficient endocytosis.

Keywords Hyperthermia · Magnetic nanoparticles dose · SAR · Tumor

Y. Arum · Y. Song
Department of Mechatronic, Pukyong National University, Pusan, South Korea

J. Oh (✉)
Department of Biomedical Engineering, Pukyong National University, Pusan, South Korea
e-mail: jungoh@pknu.ac.kr

Introduction

The potency of magnetic nanoparticles (MNPs) as effective heating agents for magnetic hyperthermia has been demonstrated many years ago. Magnetic hyperthermia is based on the fact that tumor cells are more sensitive than normal tissue and significantly less able to tolerate the added stress of heat in the range of 42–45°C due to low oxygen, normal acid concentrations, and insufficient nutrients (Cavaliere et al. 1967; Dudar and Jain 1984; Halperin et al. 2007). Higher temperatures up to 56°C, which yield widespread necrosis, coagulation, or carbonization (depending on temperature), are called 'thermoablation'. Hyperthermia is advantageous in that it has fewer side effects than thermoablation, chemotherapy, or radiation, and it has been investigated for many years in the treatment of a wide variety of malignant tumors in both experimental animals and patients (Tomitaka et al. 2009).

Magnetic hyperthermia refers to the introduction of ferromagnetic or superparamagnetic particles into the tumor tissue, followed by the application of an external varying magnetic field. Superparamagnetic materials have zero remanence and transform the energy of the magnetic field into heat through two kinds of power loss mechanisms, hysteresis loss and relaxation loss which include Brownian relaxation and Neel relaxation (Ma et al. 2004; Maenosono and Saita 2006). The efficiency of the transformation of energy is strongly dependent on the strength and frequency of the magnetic field and the properties of the magnetic particles (Gazeau et al. 2008).

Recently, the use of magnetic sensitive agarose gel has been explored for hyperthermia applications (Veverka et al. 2007; Okawa et al. 2006; Salloum et al. 2008). However, the correct control of temperature has been a difficult and complicated challenge. The reason for this problem may be

explained mainly by insufficient administered heat dosage against heat loss, resulting in entire target cancer tumors not being heated up to tissue lethal temperature. The heat dose administered in tissue takes into account two factors: the heating power of magnetic material (W/g_{tissue}) that is represented by the specific absorption rate (SAR) (Jordan et al. 1993), and the amount of magnetic nanoparticles accumulated in the cancer region, which is represented by the weight of particles per unit weight of target tumor tissue ($g_{material}/g_{tissue}$) (Yamada et al. 2010). The main issue that we have to address is finding the objective heat dose values which can overcome the amount of heat loss.

In the present study, to address the issue above, we performed a systematical variation of tumor diameters and particle dosages, and then observed the heat transfer process within the agar tissue by employing a computer-controlled heat simulator. Possibilities of achieving the estimated heat dose by integrating presently available technologies are discussed.

Experimental details

Synthesis of nanoparticle

In our experiment, we used Fe_3O_4-APTMS MNPs, where the synthesis of Fe_3O_4 NPs were performed following the procedure reported by (Park et al. 2004) and APTMS-functionalized-Fe_3O_4 MNPs were prepared by the two-step silanization process reported by (De Palma et al. 2007). For the binding of APTMS, 500 mg Fe_3O_4-oleic acid NPs were dispersed in 100 ml toluene and placed in a three neck flask. Subsequently, 5 ml APTMS and 5 ml 1 M TMAH were added and stirred under inert gas at 60°C for 1 h. Precipitations were washed with toluene/methanol (1:1), and the solvent was removed under vacuum. In the second step, the solid precipitates were dissolved in 100 ml mixture of toluene/ethanol (4:1), added to 5 ml 1 M TMAH, and stirred and heated to 60°C under inert gas for 1 h. The solid precipitations were washed with the same procedure as in step one. Finally, the colloidal solution was dried under vacuum oven at 70°C for 3 h.

Characterization methods

The changes in the chemical groups present in the nanoparticles were monitored using FTIR spectrometry (JASCO FT/IR 4100, USA). Particle size was measured using TEM (JEOL, JEM-2010, Japan). Magnetic properties were measured using SQUID (Quantum Design, MPMS XL 7.0, USA).

Magnetic heating experiment

To verify the ability of heat generation by Fe_3O_4-APTMS MNPs, we used a three turn coil (diameter 45 mm) which was powered by an induction heating system (7.5 kW WI-840, DIK, Korea) that generates a magnetic field (130 Oe, 154 kHz). To confirm the actual heat dose, 3 ml Fe_3O_4-APTMS MNPs with four different concentrations of 10, 12, 15 and 17 mg/ml were placed in 35 mm cell culture dishes. Thereafter, particles were concentrated in the middle of the dish by applying permanent magnet. After removing water, 3 ml agarose gel (1.2%) was added to each dish. Samples were put in the middle of working coil and temperatures at the upper surface of agar (5 mm from the center of the MNPs) were measured by infrared thermal imaging camera (FLIR 128 System, USA) during the experiment. To investigate heat distribution in agar tissue, the results were compared by heating sample without agar gel.

Measurement of heating potential of Fe_3O_4-APTMS represented by SAR

The magnitude of the SAR represents the heating power of particles and defined according to (Hilger et al. 2002) as

$$\mathrm{SAR}\,[\mathrm{Wg}^{-1}(\mathrm{Fe_3O_4\text{-}APTMS})] = \frac{C_{\mathrm{gel}}}{x}\frac{\mathrm{d}T}{\mathrm{d}t} \quad (1)$$

where the specific heat of agarose gel C_{gel} is assumed to be equal to the specific heat of water, i.e. 4.18 J/g °C, and dT (°C)/dt (s) is the initial 30 s slope of the temperature versus time curve. x is the weight fraction of magnetic elements in gel according to the formula

$$x = \frac{m(\mathrm{sample\ Fe_3O_4{-}APTMS})}{m(\mathrm{H_2O}) + m(\mathrm{agarose})} \quad (2)$$

where m are the masses of Fe_3O_4-APTMS, H_2O and agarose, respectively.

Cytotoxic effect of heat at different temperature generated by induction heating

Hyperthermic treatment of cultured cells was performed by heating four cell pellets at various temperatures (38, 42, 55, and 68°C) for 10 min by direct immersion in a temperature-controlled water bath. Each heated cell pellet was plated in a 60-mm cell-culture dish at the concentration of 1×10^4 cells/dish and cultured for 7 days. The number of viable cells was evaluated by the trypan blue dye exclusion method using a hemocytometer and was counted on days 1, 3, and 7. The data values and bars represent the mean and SD of three independent experiments.

Cell viability assay using WST-1

The cytotoxicity of Fe_3O_4-APTMS MNPs was measured using the WST-1 assay (ITSBio, Korea). HeLa cells were seeded at a density of 1×10^5 cells/well in 96-well plates and incubated for 24 h. Fe_3O_4-APTMS with concentration 10, 12, 15, and 17 mg/ml were added into the culture media in the plate. Untreated cells were used as controls. Cells were incubated in a humidified 5% CO_2 environment at 37°C for 12, 24, and 48 h, respectively. At the end of the incubation time, 10 µl WST-1 solution was added to each well. After 4-h incubation, plate was shaken for 1 min and absorbance was measured using a microtiter plate reader (Vmax, Molecular Device, USA) at 450 nm. Percentage cell viability was calculated by

$$\text{Cell viability} = \frac{\text{mean test wells}}{\text{mean control wells}} \times 100\% \quad (3)$$

Cell labeling using FITC

Fe_3O_4-APTMS MNPs were dispersed in 2 mL of ethanol, and 0.1 mL FITC solution (1 mg/mL in DMSO) was added to this solution. After shaking for 12 h in the dark, FITC-conjugated Fe_3O_4-APTMS was obtained by washing with ethanol and water and finally dispersed in water. Subsequently, 1 ml of FITC-conjugated Fe_3O_4-APTMS (1 mg/ml) was added to HeLa cells (1×10^5 cells/ml), which were pre-cultured on a 12-well plate for 24 h at 37°C. After 24-h exposure, the growth media was removed and the cells were washed with PBS. Then, the cells were re-incubated with a PBS solution with 3.7% formaldehyde. FITC-conjugated Fe_3O_4-APTMS and cell nucleus were monitored using fluorescence microscope.

Loss power density evaluation

Given the extrinsic (i.e., shape, diameter) and intrinsic (i.e., magnetization) properties of the particles and the intensity value of the exciting magnetic field, a specific MATLAB procedure was developed to obtain an estimate of the effective power density (W/m^3) originating from the considered magnetizing fluid. For a monodisperse solution, this power is given by, (Rosensweig 2002):

$$P = \pi\mu_0\chi_0 H_0^2 f \frac{2\pi f\tau}{1+(2\pi f\tau)^2} \quad (4)$$

In this equation μ_0 is the permeability of free space, $4\pi \times 10^{-7}$ Tm/A, H_0 and f are the amplitude and the frequency of alternating magnetic field, $\chi_0 = \mu_0 M_s^2 V/(k_B T)$, M_s is the saturation magnetization, V is the particle volume, and k_B is the Boltzmann constant. The effective relaxation time is given by $\tau^{-1} = \tau_N^{-1} + \tau_B^{-1}$, where τ_B and τ_N are the Brownian and Néel relaxation time, respectively. Brownian relaxation τ_B is neglected because it is $\sim 10^3$ times larger than the Neel relaxation time τ_N in agar gel (or in living tissue) that has large viscosity (Okawa et al. 2006), where τ_N equals

$$\tau_N = \frac{2\sqrt{KV/k_B T}}{\sqrt{\pi}\tau_0 \exp(KV/k_B T)} \quad (5)$$

K is the anisotropy constant and $\tau_0 \sim 10^{-9}$ s.

Computer-based model of heat transfer in biological tissues

Using COMSOL Multiphysics ver 3.5, we intended to compute the spatial temperature distribution within the tissues. For our problem, the temperatures are dependent on time and there is no fluid flow. The only mode of heat transfer is by conduction. So the problem is a transient conduction problem with no convection, the governing equation that needs to be solved is

$$\rho C_p \frac{\partial T}{\partial t} - \nabla(\kappa \nabla T) = Q \quad (6)$$

where ρ is the density (kg/m^3), C_p the molar specific heat at constant pressure (J/kg/°C), T the temperature (°C), t the time (s), κ the thermal conductivity (W/m/°C), Q the heat generation rate (W/m^3), and ∇ means Laplacian. The 3D symmetry model consists of a polystyrene cell-culture dish with 1-mm thick walls, 5-mm thick homogenous agar tissue layer and NPs which were located in the center of the dish and on the bottom side before the agar tissue layer. Fe_3O_4-APTMS MNPs with four different concentrations (10, 12, 15 and 17 mg/ml) were modeled as a sphere with 0.5-mm thick wall and each concentration has different diameter size (see Table 1). The physical properties of the materials are presented in Table 2. Following our experiment, the investigation was focused on the upper surface of the agar where the verification of heat generation was occurred by IR thermal imaging camera and it can only be done on the upper surface of the agar.

The initial temperature was set at 20°C. All surfaces of the plate dishes were adjusted using initial temperature except the bottom surface. Moreover, the thermal insulation was applied on the agar surface and the surfaces along

Table 1 Loss power density values of four different concentrations Fe_3O_4-APTMS MNPs

Concentration (mg/g$_{tissue}$)	Fe_3O_4-APTMS diameter region (mm)	Loss power density, P (W/m^3)
10	8.2	2.07×10^6
12	10.0	4.99×10^6
15	11.0	6.26×10^6
17	12.6	8.38×10^6

Table 2 Physical properties of material applied in computer-based simulation

Physical properties	Fe_3O_4-APTMS[a]	Agar tissue[b]	Polystyrene[c]
Heat capacity (J/kg °C)	670	4,183	1,300
Thermal conductivity (W/m °C)	6	0.6072	0.08

[a] (Maenosono and Saita 2006)

[b] (Veverka et al. 2007)

[c] (Chen et al. 2001)

the symmetry line. The heat source was addressed on the MNPs regions. In this study, the analysis time was set in 1,200 s. The models were constructed using tetrahedral element. The UMFPACK direct solver and adequate conditions needed for each calculation were automatically selected by COMSOL.

Results

Fe_3O_4-APTMS MNPs characteristic

As previously established, Fe_3O_4 MNPs in the presence of surfactants such as oleic acid are stable in non-polar solvents (such as hexane) and capped with non-polar endgroups on their surface (Jana et al. 2007). Therefore, to increase the biocompatibility of MNPs, ligand exchange was needed to tune surface properties to hydrophilic. Alkylsilanes was the best candidate for its effectiveness and simplicity in conducting the exchange of hydrophobic ligands on Fe_3O_4 MNPs and stabilization of nanoparticles (De Palma et al. 2007). The typical FT-IR spectra of Fe_3O_4 MNPs are shown in Fig. 1a. The C=O at 1,711 cm^{-1}, the C–H stretch at 2,911 cm^{-1}, and the CH_2/CH_3 bending at 1,464 cm^{-1} are

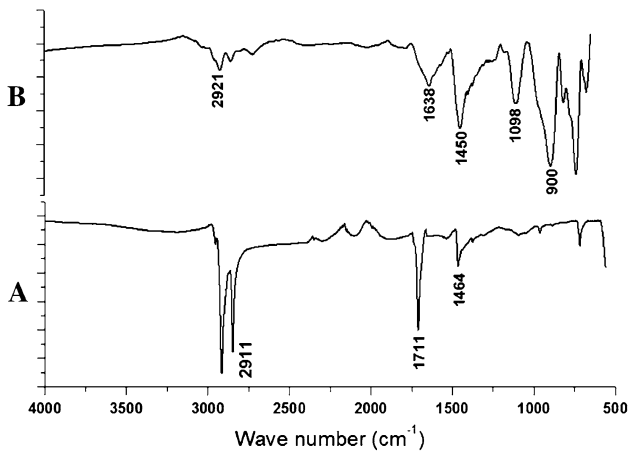

Fig. 1 The FT-IR spectra of Fe_3O_4-oleic acid (**a**) and Fe_3O_4-APTMS (**b**)

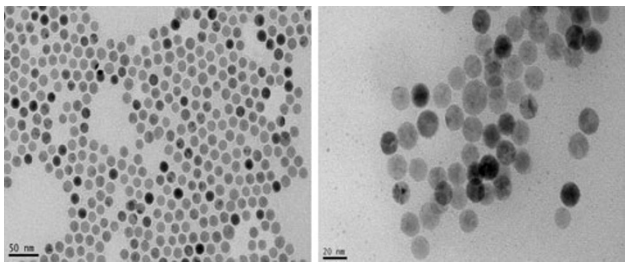

Fig. 2 TEM images Fe_3O_4-oleic acid (*left*) and Fe_3O_4-APTMS (*right*)

evidence of oleic acid-coated Fe_3O_4 MNPs. The FT-IR spectra of Fe_3O_4-APTMS, see Fig. 1b, showed the peaks around 1638 cm^{-1} ascribed to the $–NH_2$ terminal of APTMS, the CH_2 bending was found at 1,450 cm^{-1}, the C–H stretch at 2,921 cm^{-1}, the Si–O–Si bridges were seen at 1,098 cm^{-1}, and the Si–O bound at 900 cm^{-1}. The absence of oleic acid peaks replaced by silane peaks in the Fe_3O_4 MNPs, indicates that ligand exchange was successfully done.

TEM micrographs of Fe_3O_4-APTMS are shown in Fig. 2. The results suggested that ligand exchange process did not have significant effect on the particle size, both Fe_3O_4-oleic acid and Fe_3O_4-APTMS MNPs had particle size approximately 14 nm. It also can be seen that particles were spherical in shape with a narrow size distribution and uniform physico-chemical properties.

The SQUID data in Fig. 3 show the magnetic curves as function of applied field at 300 K. The saturated magnetization of Fe_3O_4-APTMS MNPs was about 38.4 emu/g, which was lower than those of Fe_3O_4-oleic acid was about 57 emu/g. Moreover, the remanence (M_r) and coercivity (H_c) were close to zero, exhibiting the characteristic of

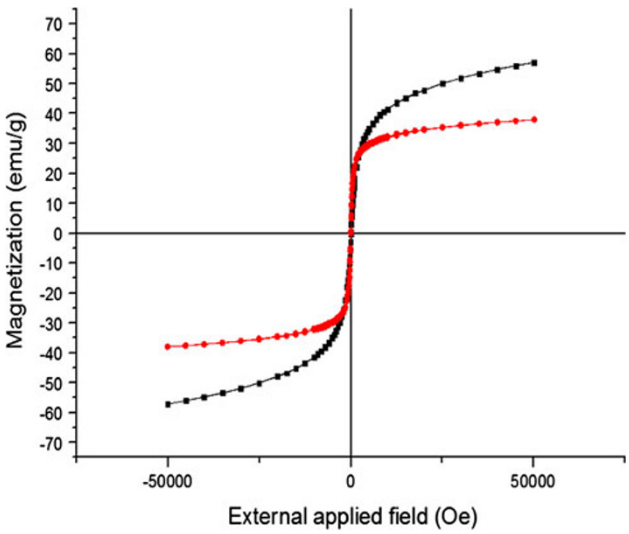

Fig. 3 Magnetic hysteresis for Fe_3O_4-oleic acid (*filled square*) and Fe_3O_4-APTMS (*filled circles*), measured at room temperature

supramagnetism. Decrease of magnetization was related to the high magnetocrystalline anisotropy of Fe_3O_4 in the presence of APTMS, which formed polymerized multilayers that suppress a tendency to destabilize magnetic ordering.

Increase of temperature in agar tissue containing Fe_3O_4-APTMS MNPs when exposed to the magnetic field

Figure 4 summarizes the results of our in vitro experiment using 1.2% agar in a polystyrene cell culture dish containing 10, 12, 15, and 17 mg Fe_3O_4-APTMS MNPs/g_{tissue}. When exposed to the magnetic field, the temperature increased sharply. Within 20 min, T_c (maximum self-controlled temperature at the center of particle) for Fe_3O_4-APTMS MNPs was 38.4, 42.6, 55.1, and 68.1°C, respectively. Meanwhile, the upper surface temperatures of agar tissue, at the region 5 mm from a center of the MNPs sphere where observed to be lower than T_c of 34.5, 38.6, 49.1, and 61.4°C, respectively. These decreases were caused by heat losses of the system.

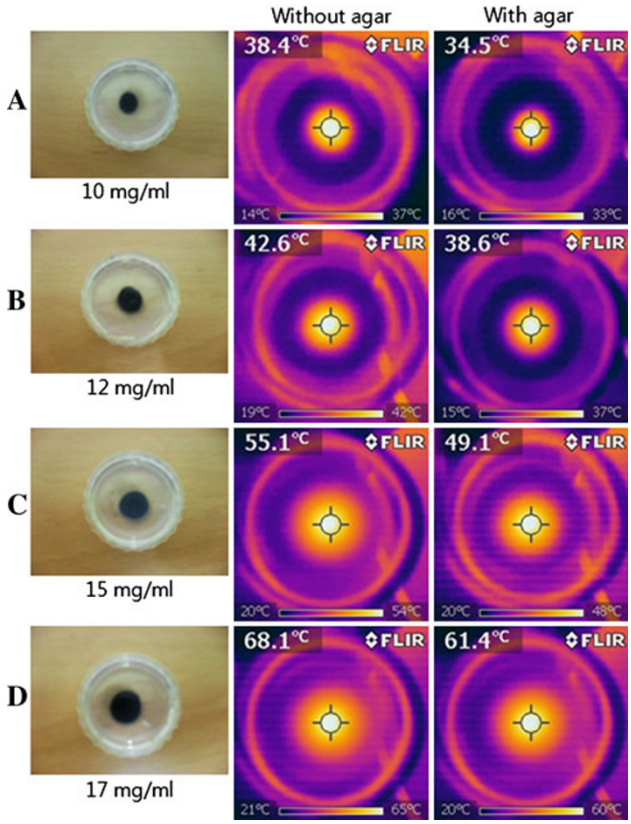

Fig. 4 Thermal response in agar surface. Temperature was observed using IR camera. To show the heat transfer process in agar gel, temperature was measured with and without agar. Fe_3O_4-APTMS MNPs were concentrated in the middle using magnet with four different concentrations **a** 10 mg/ml, **b** 12 mg/ml, **c** 15 mg/ml, and **d** 17 mg/ml. The increase of temperatures was found to be proportional to the quantity of the particles

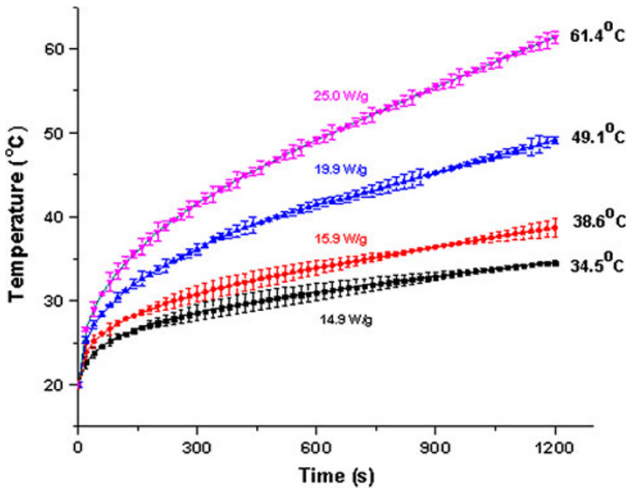

Fig. 5 Equilibrium temperatures based on experiment at the region of 5 mm from a center of the Fe_3O_4-APTMS MNPs sphere shown 34.5, 38.6, 49.1, and 61.4°C, respectively. *Error bars* represent standard deviations

Heat doses used to agar tissue phantoms in vitro to various equilibrium temperatures

To illustrate SAR as a function of MNPs content, their values are plotted in Fig. 5. Since the nanoparticles are the only heating sources present in the agar tissue, the SAR distribution can be used as an index for the particle concentration in the gel. The temperature curve at upper surface 5 mm away from the center of the MNPs is used to determine the SAR values based on Eq. 1. For magnetic field strengths 130 Oe, the SAR value was sensitive to the concentration of Fe_3O_4-APTMS MNPs. 10 mg Fe_3O_4-APTMS/g_{tissue} corresponds to an applied heat dose of 14.9 W/g_{tissue}. Similarly, 12, 15, and 17 mg Fe_3O_4-APTMS/g_{tissue} corresponds to an applied heat dose of 15.9, 19.9, 25.0 W/g_{tissue}, respectively. Herein, we obtained some insight into the observed variation value of SAR. It enables good automatic temperature control throughout the tumor as a result of the self-regulating nature of the thermosensitive materials. Moreover, the heat dose required to increase the temperature of an in vitro tissue phantom model up to 50°C is in the range 19–25 W/g_{tissue}.

Loss power density estimation and temperature prediction

The estimated hysteresis power loss values were then used as the heat source inside the agar tissue and the resulting temperature rise in the whole hepatic region was evaluated with COMSOL. Each concentration of MNPs was distributed in one spherical region whose diameter size was depended on the amount of concentration. Calculating with

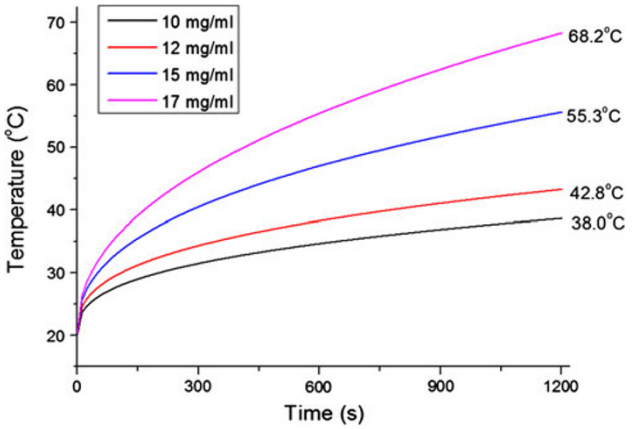

Fig. 6 The time-dependent change in the temperature of Fe_3O_4-APTMS MNPs obtained from computer simulation. The achieved temperature within 20 min for samples with concentration of 10, 12, 15, and 17 mg Fe_3O_4-APTMS/g_{tissue} were 38.0, 42.8, 55.3, 68.2°C, respectively

field magnitude H of 10.4 kA/m (130 Oe), frequency f of 154 kHz, and magnetization M 38.4 Am^2/kg, the loss power value of each spherical region is presented in Table 2. The time-dependent changes in the temperature of Fe_3O_4-APTMS MNPs heating are shown in Fig. 6. The achieved temperature within 20 min for samples with concentration of 10, 12, 15, and 17 mg Fe_3O_4-APTMS/g_{tissue} were 38.0, 42.8, 55.3, and 68.2°C, respectively. Our simulation showed close agreement to our experiment in Fig. 4b. Further, the simulation results showed that in the superparamagnetic behavior, the concentration of the particles is much more significant in determining the amount of generated heat, as opposed to the parameters of field amplitude and frequency.

Simulation of thermal gradient in vitro agar tissue phantom

Figure 7a shows 3D thermal gradient simulation in agar phantoms with Fe_3O_4-APTMS MNPs as heat source. The resulting curves of achieved temperature in the x–z plane at 5 mm distance from it using a concentration of MNPs are shown in Fig. 7b. When a heat dose of 14.9, 15.9, 19.9, and 25.0 W/g_{tissue} were administrated, the temperature at the centre of tissue increased to 34.0, 38.1, 48.8, and 61.0°C, respectively. These simulation data were quite comparable to actual experimental data (Fig. 4), indicating the validity of the COMSOL Multiphysics simulation results. To obtain temperature higher than of 42.5°C, concentration of Fe_3O_4-APTMS MNPs of 15 mg/g_{tissue} has been chosen.

Cytotoxic effect of heat

The number of viable cancer cells 1, 3, and 7 days after exposure to four different temperatures is shown in Fig. 8. The growth curves indicated that HeLa cells were relatively sensitive to heating temperature. When cells were heated at temperature of 38°C, the number of cells growth decreased significantly compared with the control. Further, our results confirmed that exposure to temperature of 42°C can induce obvious cellular damage and it is agreed with previous findings (Hickey and Weber 1982; Ito et al. 2004). Moreover, exposures to temperatures of 55 and 68°C were more than enough to kill cells.

In vitro cell viability

The potential toxicity of Fe_3O_4-APTMS MNPs was demonstrated by WST-1 cytotoxicity assay. This assay is based

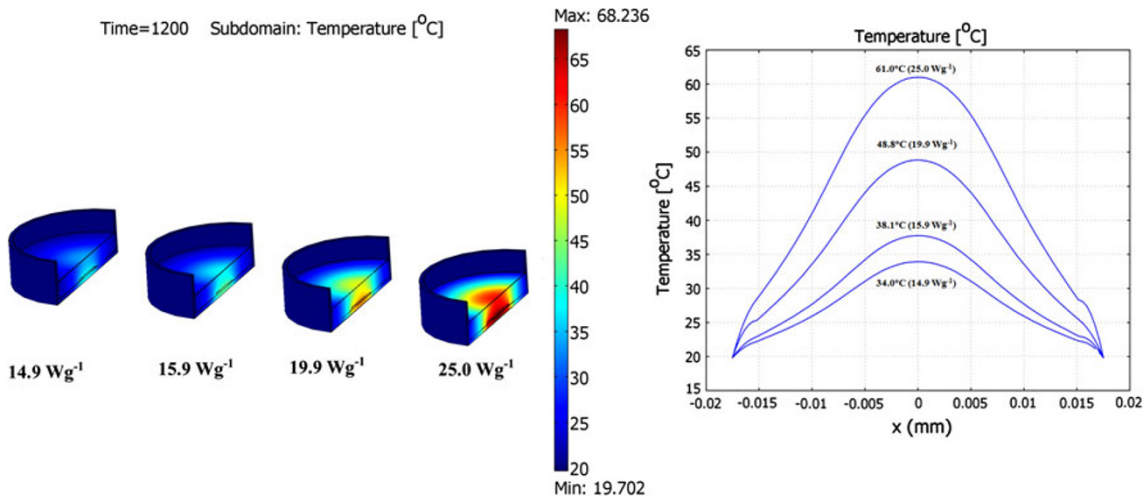

Fig. 7 Simulation of thermal gradient in agar gels (1.2%), which was heated with four different concentrations (*left*). The achieved temperature in the x–z plane at 5 mm distance from center of Fe_3O_4-APTMS MNPs spheres (*right*)

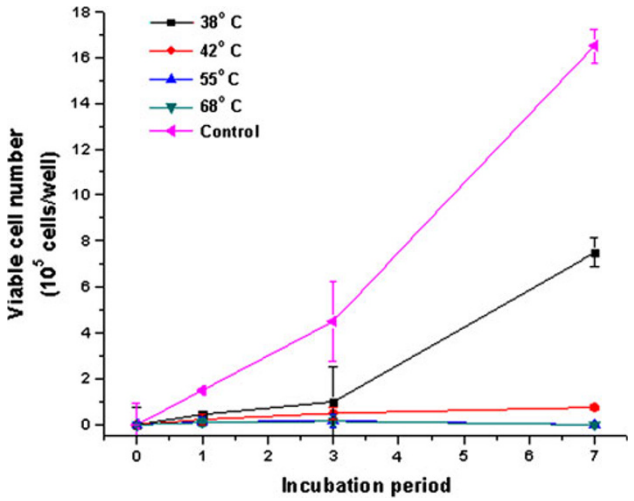

Fig. 8 Cytotoxic effect of heat treatment in HeLa cell. After 10 min exposure to various temperatures (38, 42, 55, and 68°C), each cell pellet was cultured for 7 days. The numbers of viable cells 1, 3, and 7 days after incubation were counted. The values and bars are the mean and SD of three independent experiments

on the cleavage of the tetrazolium salt into water soluble formazan by succinate-tetrazolium reductase system which belongs to the respiratory chain of the mitochondria and active only in the viable cells (Ishiyama et al. 1996). Therefore, the amount of the formazan dye is directly proportional to the number of living cells. The presence of cell viability was examined after cells were incubated for 12, 24, and 48 h. WST-1 assay indicated viability greater than 50% for all sample and were shown stable for each incubation period, see Fig. 9. It means particles did not have significant effect on cell viability and was categorized

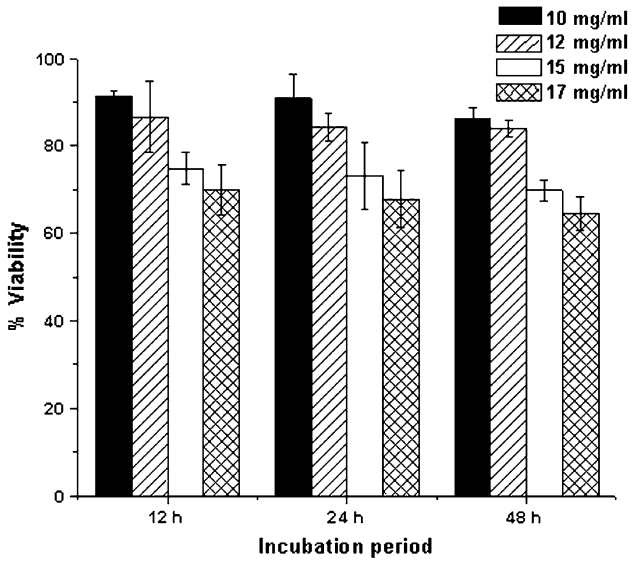

Fig. 9 In vitro cell viability of Fe_3O_4-APTMS, Fe_3O_4-APTMS-cisplatin, chitosan, CS-cisplatin-Fe_3O_4, and cisplatin in HeLa cells after 12, 24, and 48-h incubation time

as not toxic. The relationship to concentration indicates that, at the highest concentration, the cells died more quickly, and they died more slowly with decreasing concentration.

Cellular uptake of FITC-labeled Fe_3O_4-APMTS

Confocal fluorescence scanning microscope (Leica Microsystem, Germany) was used to observe the uptake of FITC-labeled Fe_3O_4-APTMS MNPs in HeLa cells after 12-h incubation is shown in Fig. 10. As shown, the fluorescence (green) areas, after 12-h exposure, the FITC-labeled Fe_3O_4-APTMS MNPs particles are present in cytoplasm. Meanwhile, the HeLa cells treated by these nanoparticles still remained large, spindle-shaped, which reveals a nice biocompatibility of the synthesized Fe_3O_4-APTMS MNPs.

Discussion and conclusion

We have developed a hyperthermia treatment protocol that makes use of Fe_3O_4-APTMS MNPs designed to produce heat for effective magnetic hyperthermia therapy. As reported earlier (Oleson et al. 1989; Andra et al. 1999), the temperature distribution is of great importance in determining how successful the treatment is. That is, how much of the tumor is heated to therapeutic temperatures, and how much of the surrounding normal tissue is damaged by the heat.

Since many years ago, in vitro investigation of heat generation in living tissue can be represented by agar, where agar gel is equivalent as heat-sensitive gels for phantom measurements and treatment verification purposes (Siddiqi 2009). In this experiment, agar tissue was used as the representative tumor to examine the amount of heat dose provided by Fe_3O_4-APTMS MNPs. According to our experimental result, for local magnetic hyperthermia using Fe_3O_4-APTMS MNPs, a concentration of 12 mg/g tissue and a SAR value 15.9 W/g tissue can be chosen. But a large tumor with diameter more than 5 mm, may be treated by applying heat dose of 19.9 W/g tissue, which resulted from concentration of 15 mg/g tissue.

Before using the software COMSOL for present heat simulation, we confirmed its reliability by comparing the data obtained by using it with the experimental data. The value of the loss power density is the basic input parameter for COMSOL. The results showed that in the superparamagnetic behavior, the concentration of the particles is much more significant in determining the amount of generated heat, as opposed to the parameters of field amplitude and frequency. However, to obtain the same size for the optimum temperature region for the same concentration of

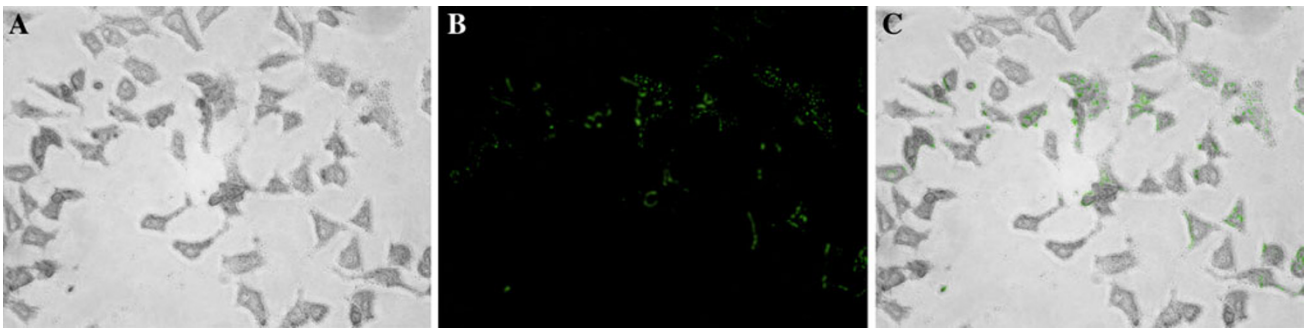

Fig. 10 Microscope images of HeLa cells after incubated with FITC-labeled Fe_3O_4-APTMS MNPs for 12 h. **a** Bright field represents phase contrast, **b** green channel of fluorescence, and **c** overlay

nanoparticles as in the superparamagnetic regime, we observed that the field amplitude and frequency must be significantly increased (Ang et al. 2007). By entering value of magnetic field of 130 Oe (at 154 kHz) into COMSOL, the simulated temperature at the center of sphere MNPs (Fig. 6) was observed to be well correlated with those detected experimentally (Fig. 4b). This result indicates that COMSOL can be used in future studies for simulation of temperatures in vivo.

The transfer of thermal energy in living tissues is a complex process which involves both metabolic heat and blood flow. For example, the blood flow within the tissue is increased by thermoregulation to remove the heat supply (Lyons et al. 1989; Pennes 1998), therefore the cooling effect of blood flow should also be taken into consideration in a clinical setting (Foster et al. 1978; Liu and Chen 2009). It is true that the presence of blood flow acts as a heat radiator and disrupts heating the tumor, however, we eliminated blood flow issue from our estimation since this obstacle may be overcome by employing a surgical technique known as Pringle's manoeuvre (Pringle 1908) which temporally occludes hepatic vascular inflow. The efficacy of Pringle's manoeuvre in reducing heat loss has been clinically shown in radio-frequency ablation treatment (Percivale et al. 2004). We therefore focused only on static thermal diffusion loss to surrounding tissues as a heat loss factor.

To define the required temperature for cancer cell killing, we demonstrated the influence of heating treatment on cells growth. Since heat sensitivity of clinical cancers is known to be variable, we used cell pellet to represent the hard tumor tissue following the previous methods (Shinkai et al. 1996; Yamada et al. 2010) and it was found that HeLa cells are relatively sensitive to heating temperature. We applied the treatment time at 10 min, since long irradiation of AC magnetic field to living body tissue causes adverse events (Ivkov et al. 2005). Our results (Fig. 8) demonstrated that maintaining a temperature of 42°C for 10 min was insufficient and resulted in the reproliferation of cancer cells, while a temperature of 55°C maintained for 10 min resulted in complete cell death regardless of the heat sensitivity of each cell type.

Cytotoxicity measurements were originally designed for rapid and inexpensive analysis of soluble pharmaceuticals. They are also useful in the initial development of novel nanoparticle formulations. As these results demonstrate, the particular cytotoxicity assay selected could produce erroneous findings due to nanoparticle-assay interference, and thus careful experimental design is required to detect potential interactions. In this study, WST-1 assays were used to quantify cellular viability, rather than the formazan product generated in the MTT assay (L'Azou et al. 2008). When we applying MTT, Fe_3O_4-APTMS MNPs were soluble in DMSO and it caused interferences in measurement. Therefore, to avoid that, we assessed MNPs potential cytotoxicity using WST-1 assay (Lu et al. 2006; Xu et al. 2008). According to our experimental data in Fig. 9, the viability cells showed more than 50% for all concentrations and these values are quite stable for all incubation periods. Thus, we can ensure that APTMS surface modification of Fe_3O_4 MNPs has non-toxic effect to the cell.

Here, we also examined the feasibility of using these MNPs as an intracellular delivery carrier. FITC, an extensively used fluorescent marker (Rossi et al. 2004; Zhang et al. 2009) was used to label nanoparticles. The results clearly demonstrated that these Fe_3O_4-APTMS MNPs could serve as an efficient carrier by absorptive endocytosis into the cell cytoplasm.

In conclusion, our results show that by using these models, we can successfully estimate the impact of the particle dose on the efficiency of hyperthermia therapy. It could be thus a good method to evaluate the prospects of the therapy for a given patient who has a well-described condition and also to establish an optimum starting dose for magnetic hyperthermia therapy in such a case. Moreover, Fe_3O_4-APTMS MNPs exhibited good magnetic properties,

biocompatibility, low cytotoxicity and efficient endocytosis. Thus, based on our obtained results, it can be concluded that Fe_3O_4-APTMS MNPs will have excellent potential as novel magnetic nanoparticles for hyperthermia.

Acknowledgments This research was supported by Basic Science Research Program through the National Research Foundation of Korean (NRF) funded by the Ministry of Education, Science and Technology (2010-0016412), and a grant from the National R&D Program for Cancer Control, Ministry for Health, Welfare and Family affairs, Republic of Korea (No. 2010-0920190).

Open Access This article is distributed under the terms of the Creative Commons Attribution License which permits any use, distribution and reproduction in any medium, provided the original author(s) and source are credited.

References

Andra W, d' Ambly C, Hergt R, Hilger I, Kaiser W (1999) Temperature distribution as function of time around a small spherical heat source of local magnetic hyperthermia. J Magn Magn Mater 194(1–3):197–203

Ang K, Venkatraman S, Ramanujan R (2007) Magnetic PNIPA hydrogels for hyperthermia applications in cancer therapy. Mater Sci Eng: C 27(3):347–351

Cavaliere R, Ciocatto EC, Giovanella BC, Heidelberger C, Johnson RO, Margottini M, Mondovi B, Moricca G, Rossi Fanelli A (1967) Selective heat sensitivity of cancer cells. Biochemical and clinical studies. Cancer 20(9):1351–1381

Chen G, Liu S, Chen S, Qi Z (2001) FTIR spectra, thermal properties, and dispersibility of a polystyrene/montmorillonite nanocomposite. Macromol Chem Phys 202(7):1189–1193

De Palma R, Peeters S, Van Bael M, Van den Rul H, Bonroy K, Laureyn W, Mullens J, Borghs G, Maes G (2007) Silane ligand exchange to make hydrophobic superparamagnetic nanoparticles water-dispersible. Chem Mater 19(7):1821–1831

Dudar TE, Jain RK (1984) Differential response of normal and tumor microcirculation to hyperthermia. Cancer Res 44(2):605

Foster K, Kritikos H, Schwan H (1978) Effect of surface cooling and blood flow on the microwave heating of tissue. IEEE Trans Biomed Eng 25(3):313–316

Gazeau F, Lévy M, Wilhelm C (2008) Optimizing magnetic nanoparticle design for nanothermotherapy. Nanomedicine 3(6): 831–844

Halperin EC, Perez CA, Brady LW (2007) Perez and Brady's principles and practice of radiation oncology. Lippincott Williams and Wilkins, Hagerstown

Hickey ED, Weber LA (1982) Modulation of heat shock polypeptide synthesis in HeLa cells during hyperthermia and recovery. Biochemistry 21(7):1513–1521

Hilger I, Fruhauf K, Andra W, Hiergeist R, Hergt R, Kaiser WA (2002) Heating potential of iron oxides for therapeutic purposes in interventional radiology. Acad radiol 9(2):198–202

Ishiyama M, Tominaga H, Shiga M, Sasamoto K, Ohkura Y, Ueno K (1996) A combined assay of cell viability and in vitro cytotoxicity with a highly water-soluble tetrazolium salt, neutral red and crystal violet. Biol Pharm Bull 19(11):1518–1520

Ito A, Kuga Y, Honda H, Kikkawa H, Horiuchi A, Watanabe Y, Kobayashi T (2004) Magnetite nanoparticle-loaded anti-HER2 immunoliposomes for combination of antibody therapy with hyperthermia. Cancer Lett 212(2):167

Ivkov R, DeNardo SJ, Daum W, Foreman AR, Goldstein RC, Nemkov VS, DeNardo GL (2005) Application of high amplitude alternating magnetic fields for heat induction of nanoparticles localized in cancer. Clin Cancer Res 11(19):7093s

Jana N, Earhart C, Ying J (2007) Synthesis of water-soluble and functionalized nanoparticles by silica coating. Chem Mater 19(21):5074–5082

Jordan A, Wust P, Fähling H, John W, Hinz A, Felix R (1993) Inductive heating of ferrimagnetic particles and magnetic fluids: physical evaluation of their potential for hyperthermia. Int J Hyperthermia 9(1):51–68

L'Azou B, Jorly J, On D, Sellier E, Moisan F, Fleury-Feith J, Cambar J, Brochard P, Ohayon-Courtès C (2008) In vitro effects of nanoparticles on renal cells. Part Fibre Toxicol 5(1):22

Liu KC, Chen HT (2009) Analysis for the dual-phase-lag bio-heat transfer during magnetic hyperthermia treatment. Int J Heat Mass Transf 52(5–6):1185–1192

Lu J, Yang S, Ng KM, Su CH, Yeh CS, Wu YN, Shieh DB (2006) Solid-state synthesis of monocrystalline iron oxide nanoparticle based ferrofluid suitable for magnetic resonance imaging contrast application. Nanotechnology 17:5812

Lyons BE, Samulski TV, Cox RS, Fessenden P (1989) Heat loss and blood flow during hyperthermia in normal canine brain I: Empirical study and analysis. Int J Hyperthermia 5(2):225–247

Ma M, Wu Y, Zhou J, Sun Y, Zhang Y, Gu N (2004) Size dependence of specific power absorption of Fe_3O_4 particles in AC magnetic field. J Magn Magn Mater 268(1–2):33–39

Maenosono S, Saita S (2006) Theoretical assessment of FePt nanoparticles as heating elements for magnetic hyperthermia. IEEE Trans Magn 42(6):1638–1642

Okawa K, Sekine M, Maeda M, Tada M, Abe M, Matsushita N, Nishio K, Handa H (2006) Heating ability of magnetite nanobeads with various sizes for magnetic hyperthermia at 120; kHz, a noninvasive frequency. J Appl Phys 99:08H102

Oleson J, Dewhirst M, Harrelson J, Leopold K, Samulski T, Tso C (1989) Tumor temperature distributions predict hyperthermia effect. Int J Radiat Oncol Biol Phys 16(3):559–570

Park J, An K, Hwang Y, Park J, Noh H, Kim J, Park J, Hwang N, Hyeon T (2004) Ultra-large-scale syntheses of monodisperse nanocrystals. Nat Mater 3(12):891–895

Pennes HH (1998) Analysis of tissue and arterial blood temperatures in the resting human forearm. J Appl Physiol 85(1):5

Percivale A, Stella M, Barabino G, Pasqualini M, Pellicci R (2004) Radiofrequency thermal ablation of hepatocellular carcinoma: our five year experience. Ann Ital Chir 75(6):635–642

Pringle JH (1908) V. Notes on the arrest of hepatic hemorrhage due to trauma. Ann Surg 48(4):541

Rosensweig R (2002) Heating magnetic fluid with alternating magnetic field. J Magn Magn Mater 252:370–374

Rossi L, Quach A, Rosenzweig Z (2004) Glucose oxidase–magnetite nanoparticle bioconjugate for glucose sensing. Anal Bioanal Chem 380(4):606–613

Salloum M, Ma R, Weeks D, Zhu L (2008) Controlling nanoparticle delivery in magnetic nanoparticle hyperthermia for cancer treatment: Experimental study in agarose gel. Int J Hyperthermia 24(4):337–345

Shinkai M, Yanase M, Honda H, Wakabayashi T, Yoshida J, Kobayashi T (1996) Intracellular hyperthermia for cancer using magnetite cationic liposomes: in vitro study. Cancer Sci 87(11):1179–1183

Siddiqi AK (2009) Development of tissue-equivalent heat-sensitive gel for the experimental verification of near infrared (nir) laser-mediated cancer detection and therapy. Ph.D. thesis

Tomitaka A, Hirukawa A, Yamada T, Morishita S, Takemura Y (2009) Biocompatibility of various ferrite nanoparticles evaluated by in vitro cytotoxicity assays using HeLa cells. J Magn Magn Mater 321(10):1482–1484

Veverka M, Veverka P, Kaman O, Lancok A, Záveta K, Pollert E, Knížek K, Bohácek J, Beneš M, Kašpar P (2007) Magnetic heating by cobalt ferrite nanoparticles. Nanotechnology 18:345704

Xu C, Xie J, Ho D, Wang C, Kohler N, Walsh EG, Morgan JR, Chin YE, Sun S (2008) Au–Fe_3O_4 Dumbbell Nanoparticles as Dual Functional Probes. Angew Chem Int Ed 47(1):173–176

Yamada K, Oda T, Hashimoto S, Enomoto T, Ohkohchi N, Ikeda H, Yanagihara H, Kishimoto M, Kita E, Tasaki A (2010) Minimally required heat doses for various tumour sizes in induction heating cancer therapy determined by computer simulation using experimental data. Int J Hyperthermia 26(5):465–474

Zhang Y, Gong SWY, Jin L, Li SM, Chen ZP, Ma M, Gu N (2009) Magnetic nanocomposites of Fe_3O_4/SiO2-FITC with pH-dependent fluorescence emission. Chin Chem Lett 20(8):969–972